

Supplementary Information

Prussian blue analogues-derived high-entropy alloy nanoarchitectonics for efficient Fenton-like catalysis

Yiyuan Yao,^a Shifu Wang,^b Chaohai Wang,^a Zetong Wu,^a Chengming Xiao,^a Xin Guo,^a Xin Yan,^a Junwen Qi,^a Yujun Zhou,^a Zhigao Zhu,^a Yue Yang,^a Xuning Li,^b Jiansheng Li^{a}*

^a Jiangsu Key Laboratory of Chemical Pollution Control and Resources Reuse, School of Environmental and Biological Engineering, Nanjing University of Science and Technology, Nanjing 210094, People's Republic of China.

^b State Key Laboratory of Catalysis, Dalian Institute of Chemical Physics, Chinese Academy of Sciences, Dalian 116023, People's Republic of China.

E-mails: lijsh@njust.edu.cn

Text S1. Chemicals.

All reagents used in this experiment were of analytical grade and without further purifications. Anhydrous methanol, anhydrous ethanol, and *p*-benzoquinone (*p*-BQ) was purchased from Sinopharm Chemical Reagent Co., Ltd. *Tert*-butyl alcohol (TBA), methyl phenyl sulfone (PMSO₂), sodium chloride (NaCl), sodium bicarbonate (NaHCO₃), sodium dihydrogen phosphate (NaH₂PO₄), sodium nitrate (NaNO₃), and sodium sulfate anhydrous (Na₂SO₄) were purchased from Aladdin. Sodium persulfate (Na₂S₂O₈), phenol, *L*-histidine, methyl phenyl sulfoxide (PMSO), 2,2,6,6-tetramethyl-4-piperidone (TEMP), and 5,5-dimethyl-1-pyrroline N-oxide (DMPO) were provided by Meryer. Bisphenol A (BPA), PMS (Oxone, HKSO₅•0.5HKSO₄•0.5K₂SO₄), and 2,2'-Azinobis-(3-ethylbenzthiazoline-6-sulphonate) (ABTS) were purchased from Sigma-Aldrich.

Text S2. Catalytic Analyses.

Quantitative analysis of chemical PMSO and the oxidative product PMSO₂ using HPLC (Waters, e2695). All the samples were sure to filter through a water phase filter (0.22 μm) before analysis. The mobile phases and detection wavelengths were set with different pollutions: acetonitrile/water (20:80 v/v) with $\lambda = 215$ nm for PMSO and PMSO₂.

The concentration of PMS remaining in solution was determined by colorimetric method. About 5.0 mL of the sample was filtered through a 0.45 μm glass fiber syringe filter. Then 5 mL Mili-Q water, 0.4 mL ABTS (10 mM) and 0.2 mL Co²⁺ (10 mM) were immediately added to react for 10 min to form green ABTS free radical cations. The solution was analyzed by ultraviolet/visible spectrophotometer (UV-1800pc, Mapada) at a maximum absorption wavelength (λ_{max}) of 735 nm.¹

Text S3. Electrochemical experiments

The open circuit potential was tested by the electrochemical workstation (CHI 760D, Chenhua, Shanghai), with a three-electrode system consisting of a working electrode, an Ag/AgCl reference electrode, and a platinum sheet counter electrode. The electrolyte solution is Na₂SO₄ (10 mL, 0.1 mol L⁻¹).

Text S4. Computational Method.

All the calculations are performed in the framework of the density functional theory with the projector augmented plane-wave method, as implemented in the Vienna ab initio simulation package. The generalized gradient approximation proposed by Perdew, Burke, and Ernzerhof is selected for the exchange-correlation potential. The long range van der Waals interaction is taken into account by DFT-D3 approach. The cut-off energy for plane wave is set to 400 eV. The energy criterion is set to 10^{-5} eV in iterative solution of the Kohn-Sham equation. The Brillouin zone integration is performed at the Gamma point. All the structures are relaxed until the residual forces on the atoms have declined to less than 0.05 eV/Å. The Gibbs free energies are defined as:

$$G = E + E_{ZPE} - TS,$$

where E , E_{ZPE} , and TS refer to the total energy of the system, the zero-point energy, and the entropy.

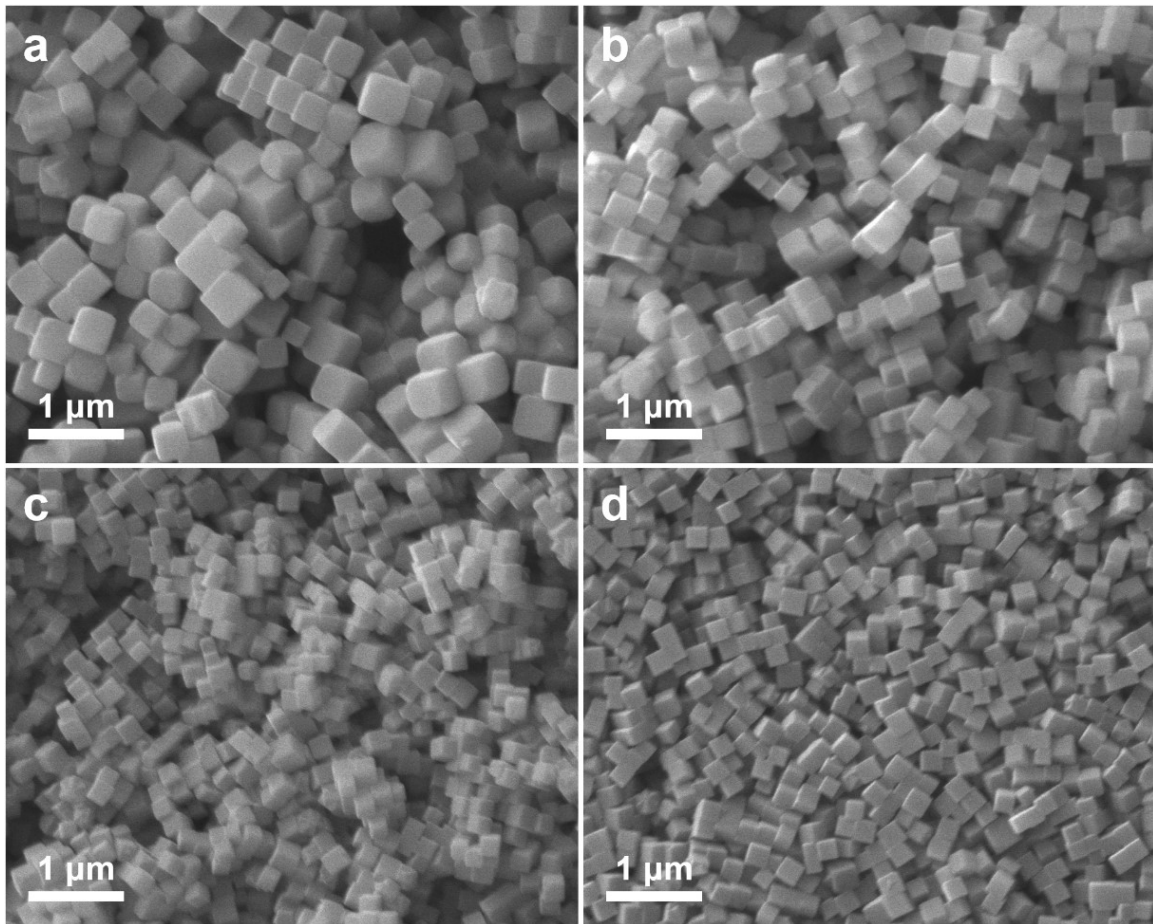


Figure S1. The SEM images of (a) FeCo-PBAs; (b) FeCoMn-PBAs; (c) FeCoMnCu-PBAs; (d) FeCoMnNiCu-PBAs.

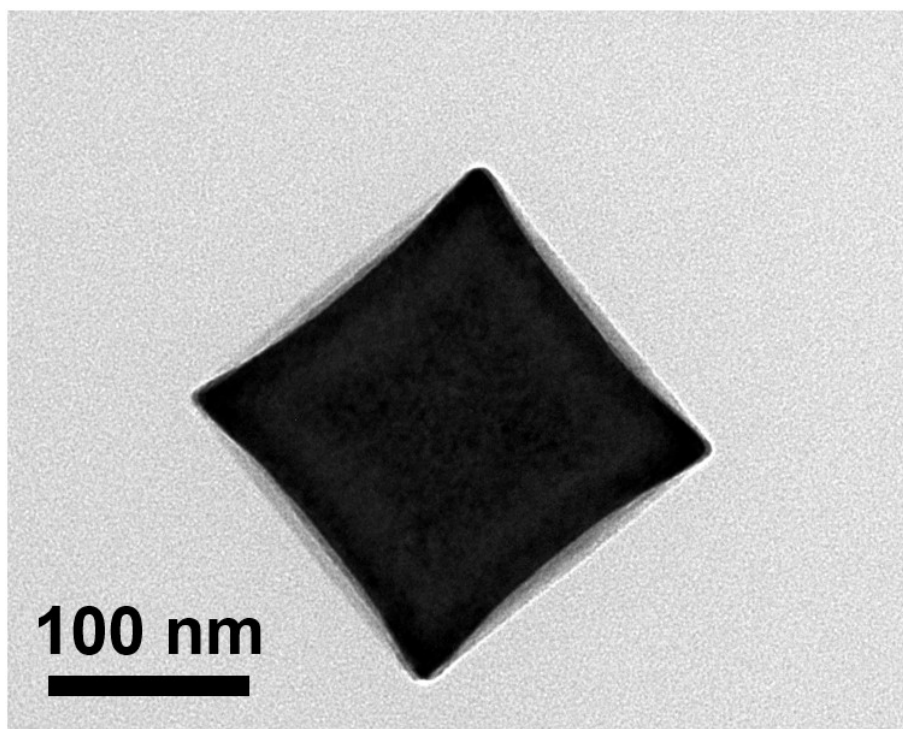


Figure S2. The TEM image of FeCoMnNiCu-PBAs.

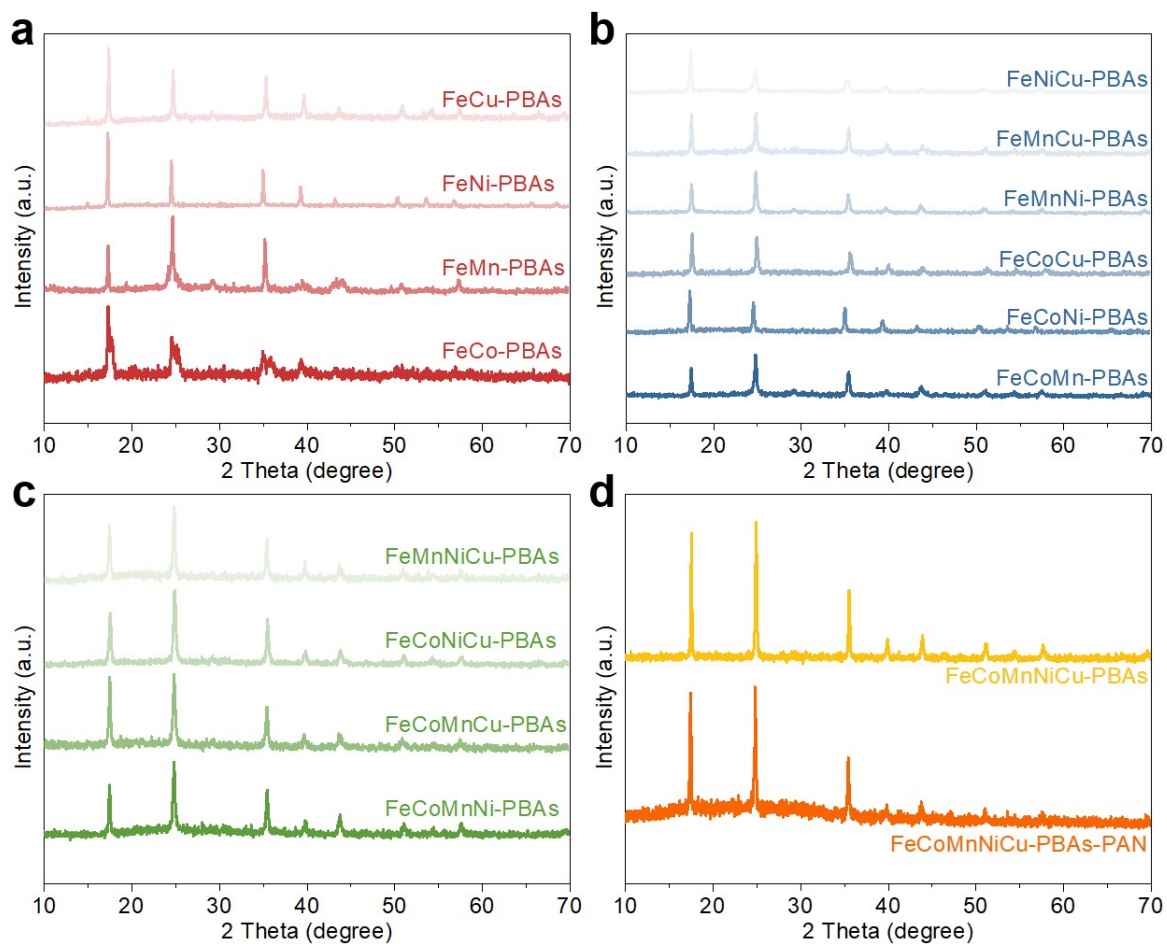


Figure S3. (a) The XRD patterns of (a) binary-PBAs; (b) ternary-PBAs; (c) quaternary-PBAs; and (d) high entropy-PBA after electrospinning.

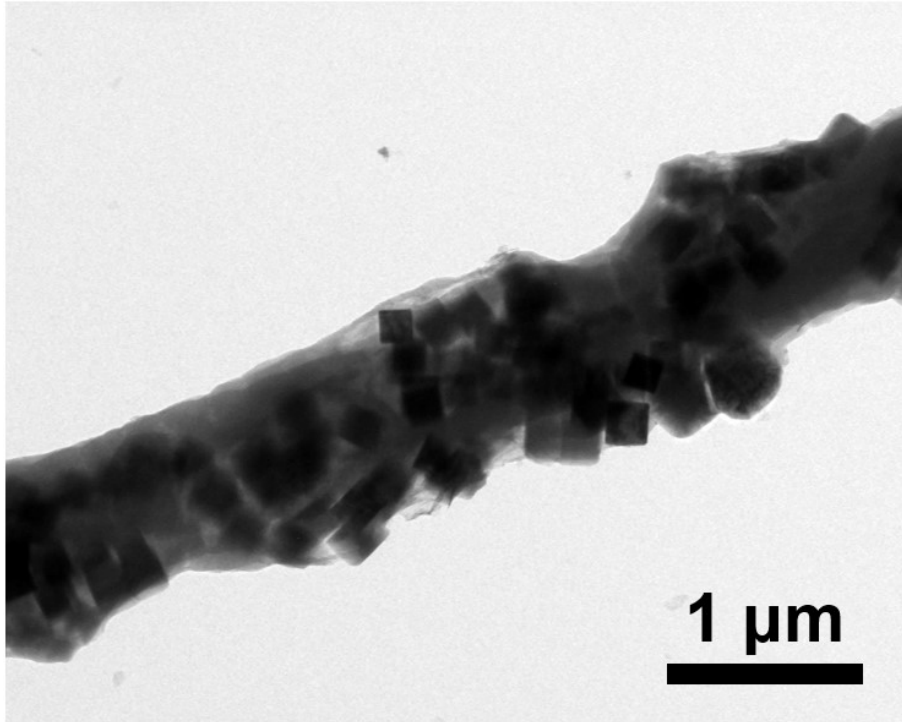


Figure S4. The TEM image of FeCoMnNiCu-PBAs-PAN.

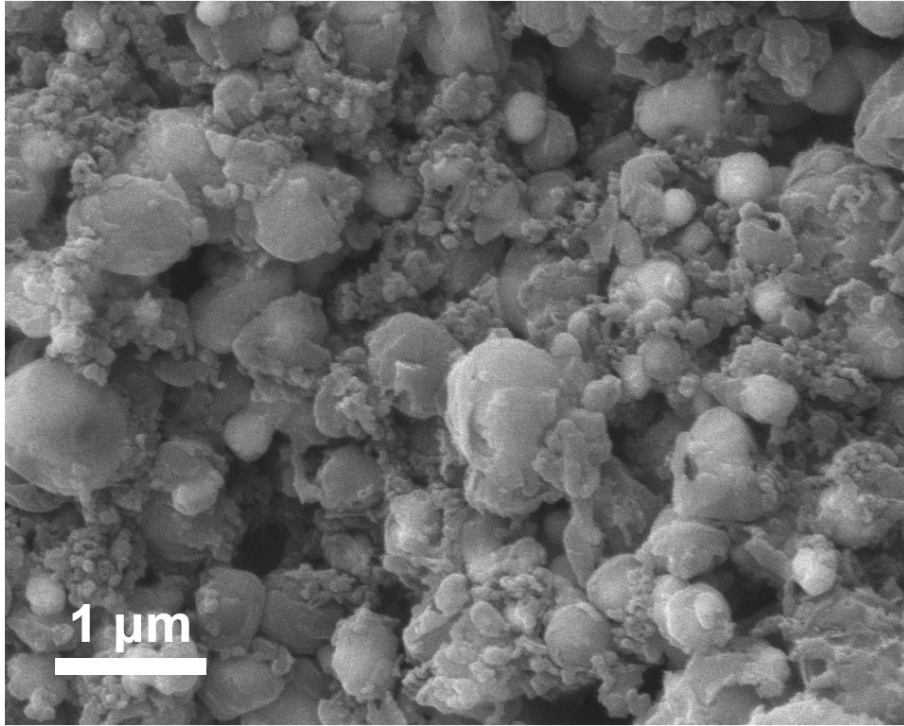


Figure S5. The SEM image of FeCoMnNiCu-PBAs-C.

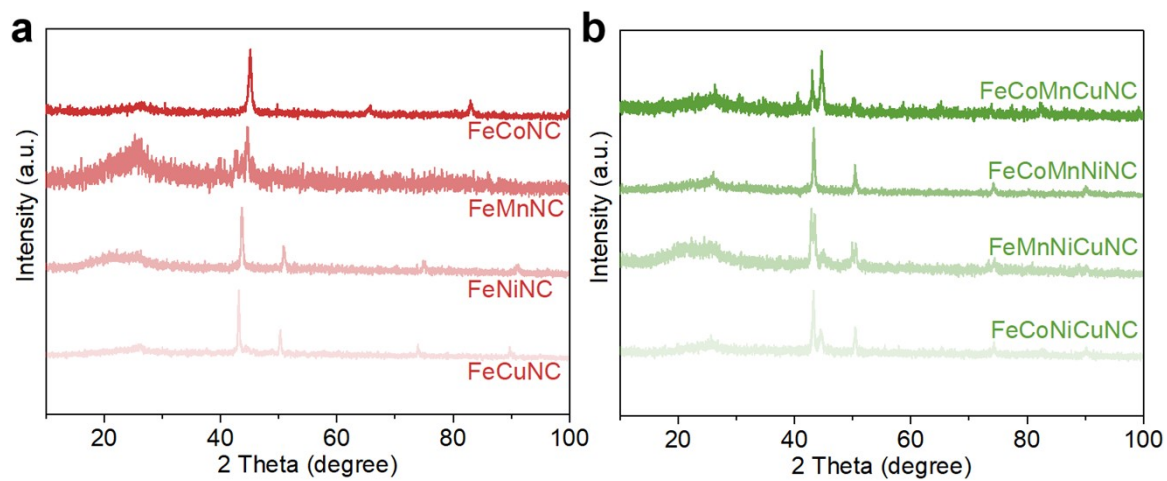


Figure S6. The XRD patterns of (a) binary NC; (b) quaternary NC.

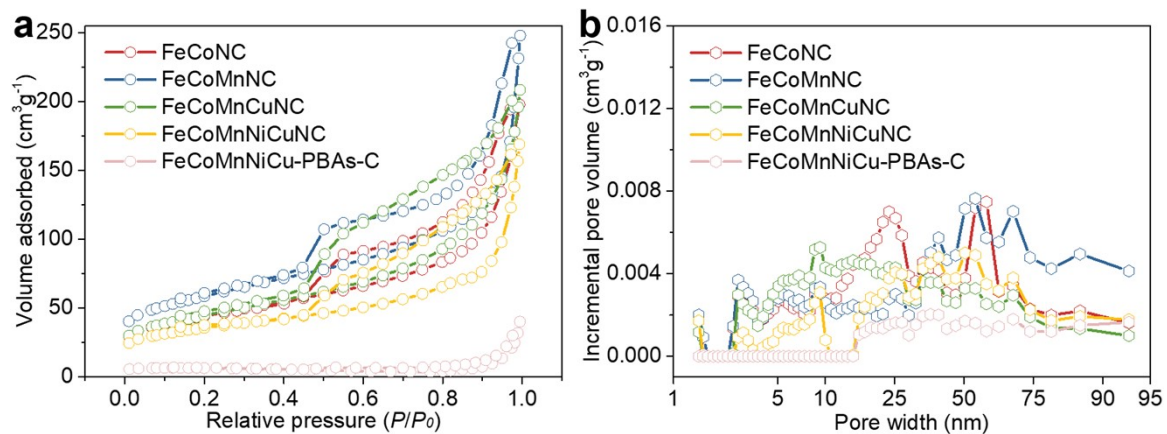


Figure S7. (a) The N₂ adsorption-desorption isotherms; (b) the pore size distribution of different samples.

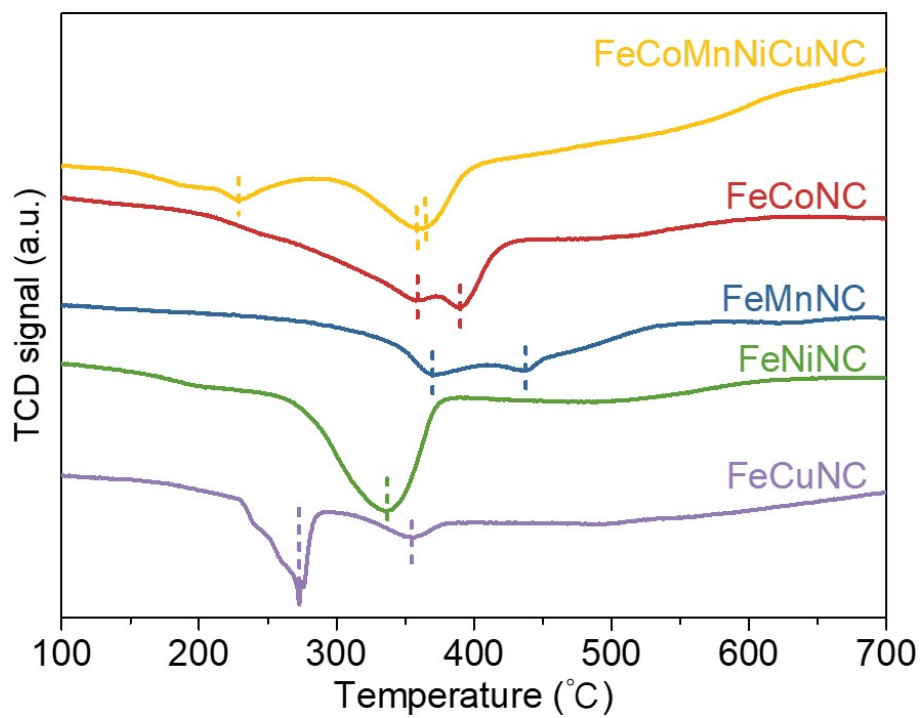


Figure S8. The H₂-TPR spectra of the different metal NC.

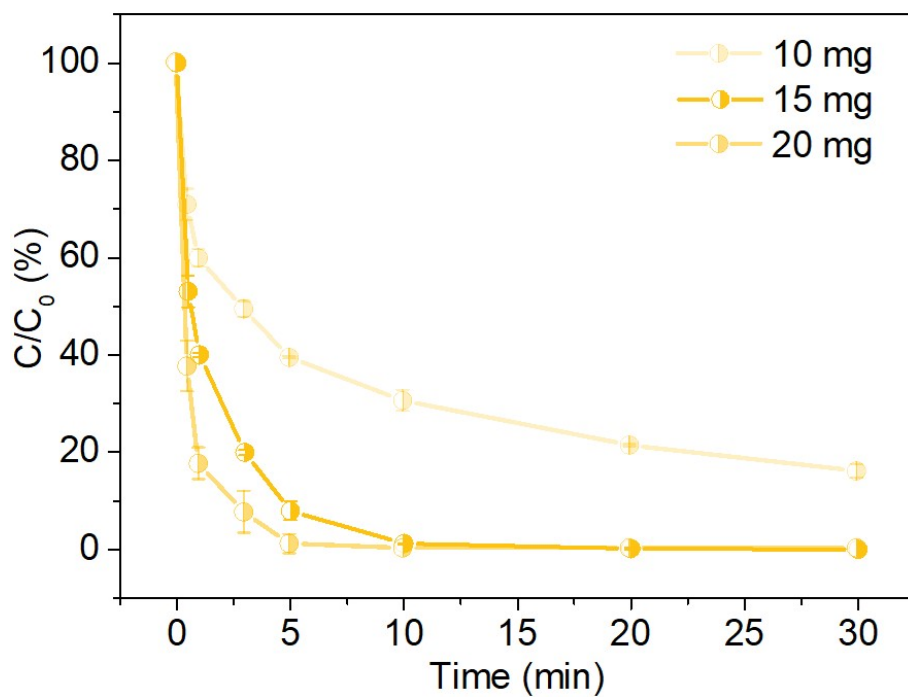


Figure S9. BPA removal in PMS-activated process of FeCoMnNiCuNC dosage. Conditions: [BPA] = 20 mg L⁻¹; [PMS] = 0.2 g L⁻¹; [Cat] = 0.15 g L⁻¹, initial pH= 3.6, T = 298 K.

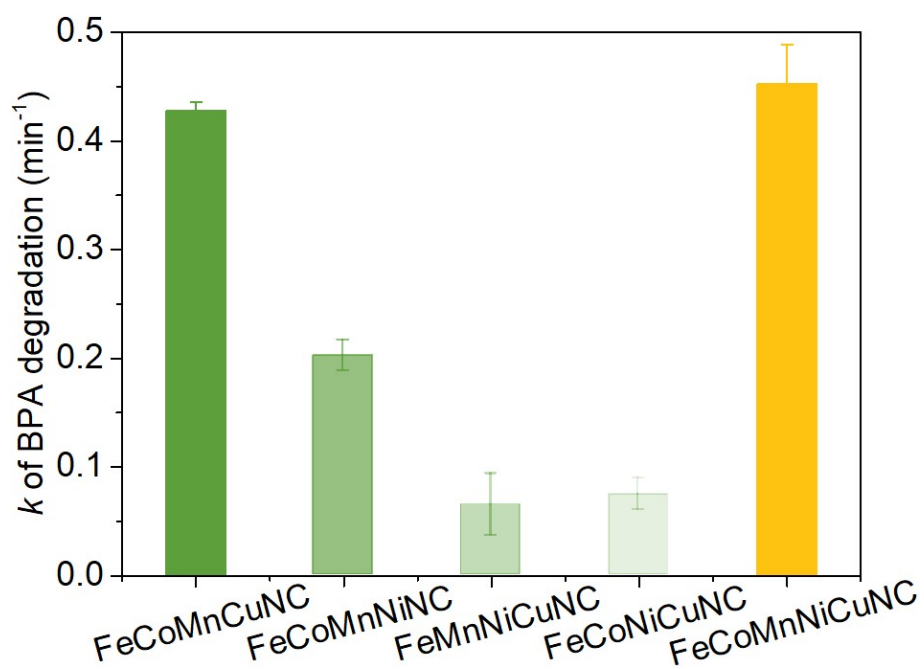


Figure S10. *k* of BPA degradation by the quaternary catalysts. Conditions: [BPA] = 20 mg L⁻¹; [PMS] = 0.2 g L⁻¹; [Cat] = 0.15 g L⁻¹, initial pH= 3.6, T = 298 K.

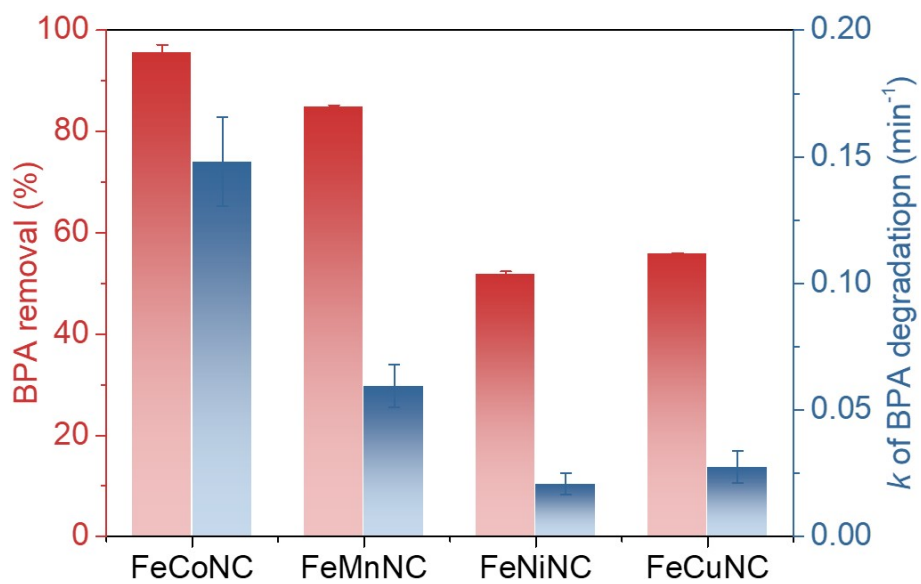


Figure S11. *k* of BPA removal in PMS-activated process by the binary catalysts. Conditions: [BPA] = 20 mg L⁻¹; [PMS] = 0.2 g L⁻¹; [Cat] = 0.15 g L⁻¹, initial pH= 3.6, T = 298 K.

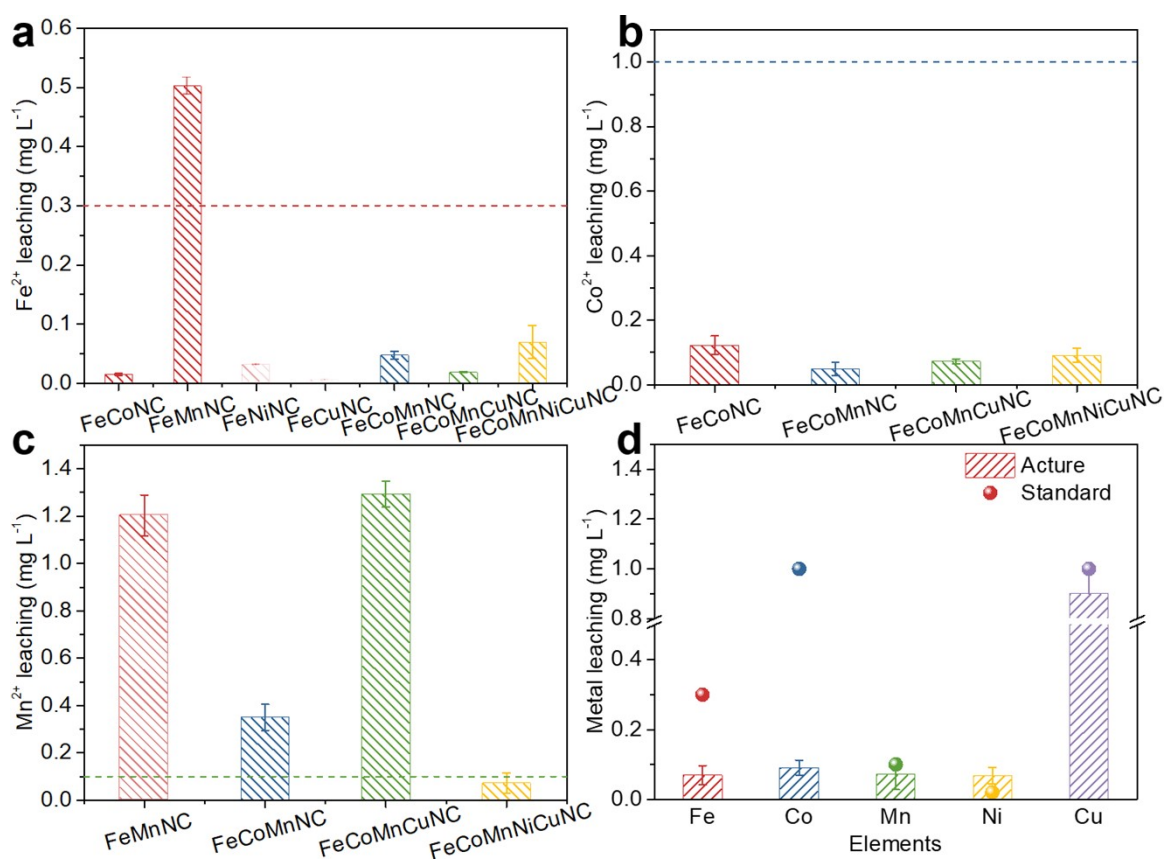


Figure S12. The metal leaching in different BPA removal systems. (a) Fe²⁺; (b) Co²⁺; (c) Mn²⁺ in different catalysts; (d) Fe²⁺, Co²⁺, Mn²⁺, Ni²⁺, and Cu²⁺ in FeCoMnNiCuNC/PMS system.

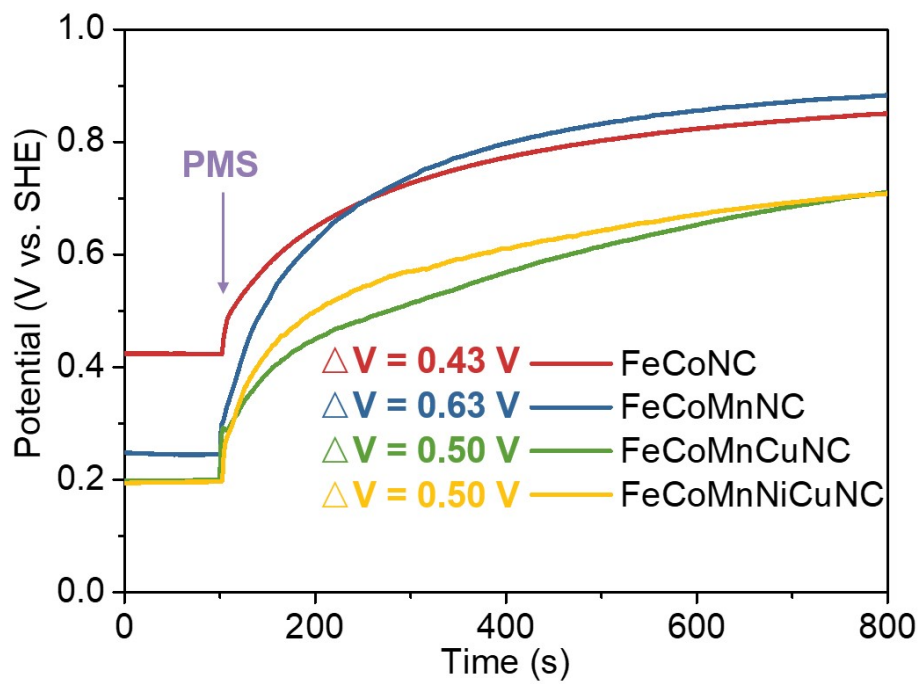


Figure S13. Open-circuit potential curves with the addition of PMS.

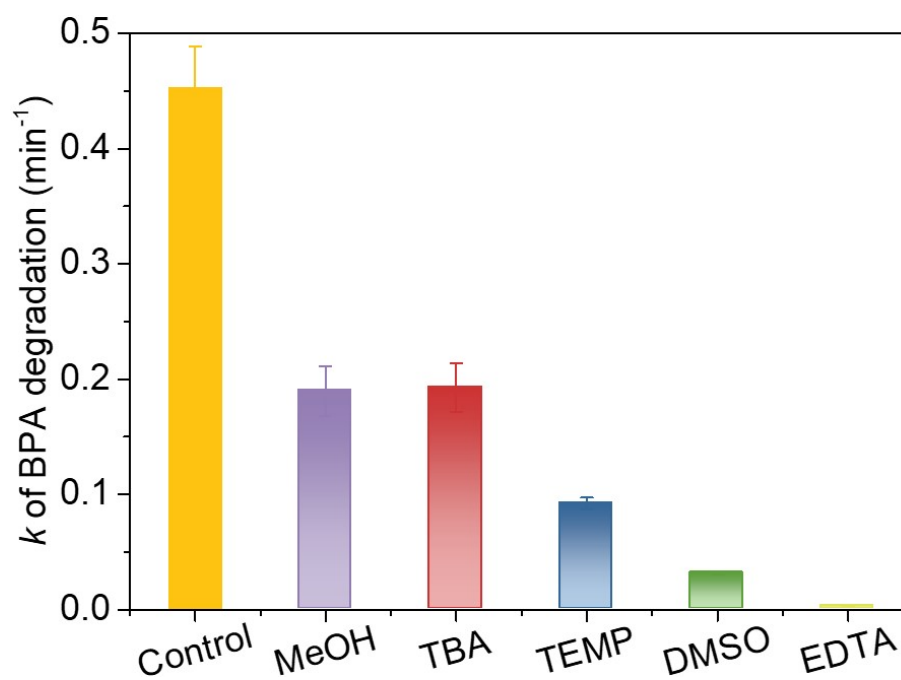


Figure S14. *k* of BPA removal in PMS-activated process by the FeCoMnNiCuNC in different quenching conditions. Reaction condition: [BPA] = 20 mg L⁻¹; [PMS] = 0.2 g L⁻¹ = 0.65 mM; [Cat] = 0.15 g L⁻¹; [MeOH] = 0.65 M; [TBA] = 0.65 M; [L-his] = 0.65 mM; [DMSO] = 0.65 mM; [EDTA] = 5 mM; [PMSO] = 20 μM; initial pH= 3.6, T = 298 K.

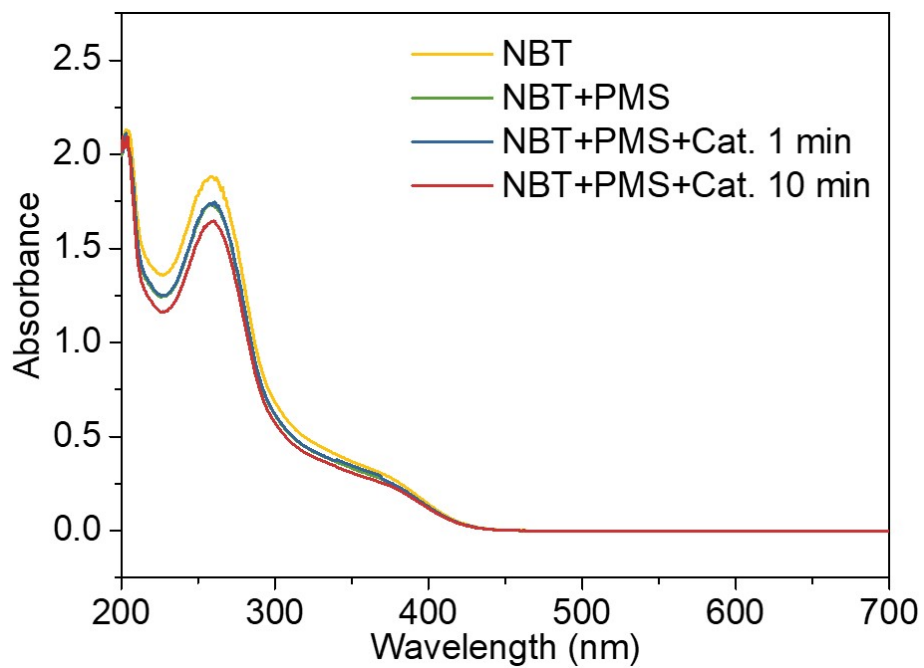


Figure S15. Quantitative determination of $O_2^{\cdot-}$ in the FeCoMnNiCuNC/PMS system. Reaction condition: $[PMS] = 0.2 \text{ g L}^{-1} = 0.65 \text{ mM}$; $[Cat] = 0.15 \text{ g L}^{-1}$; initial pH= 3.6, $T = 298 \text{ K}$.

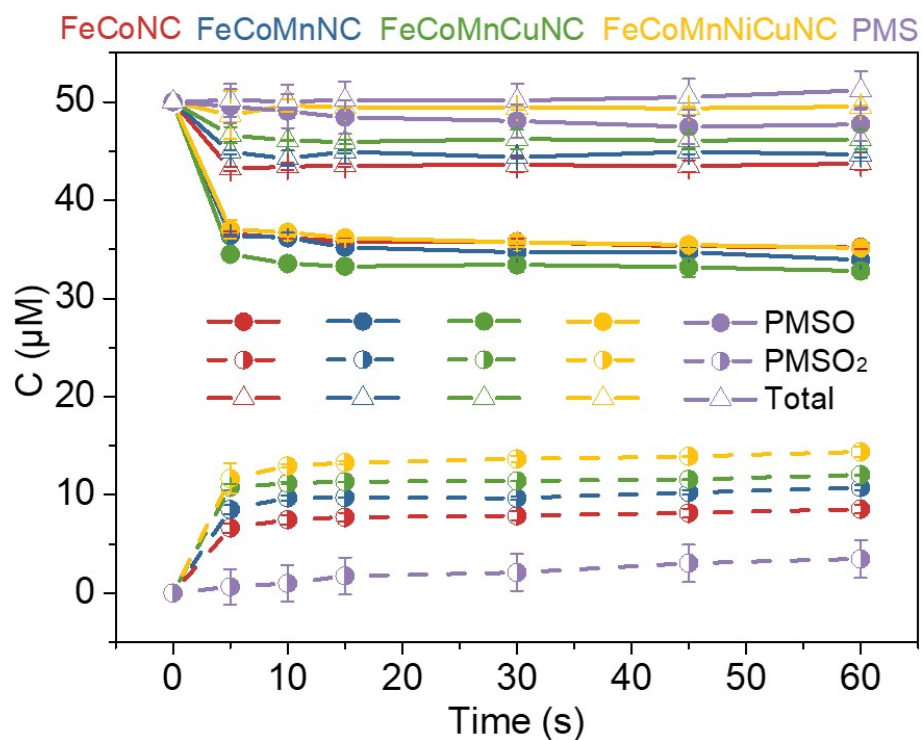


Figure S16. Efficiency of the degradation of PMSO and generation of PMSO₂ in the FeCoMnNiCuNC /PMS system. Reaction condition: [PMSO] = 50 μM; [PMS] = 0.2 g L⁻¹ = 0.65 mM; [Cat] = 0.15 g L⁻¹.

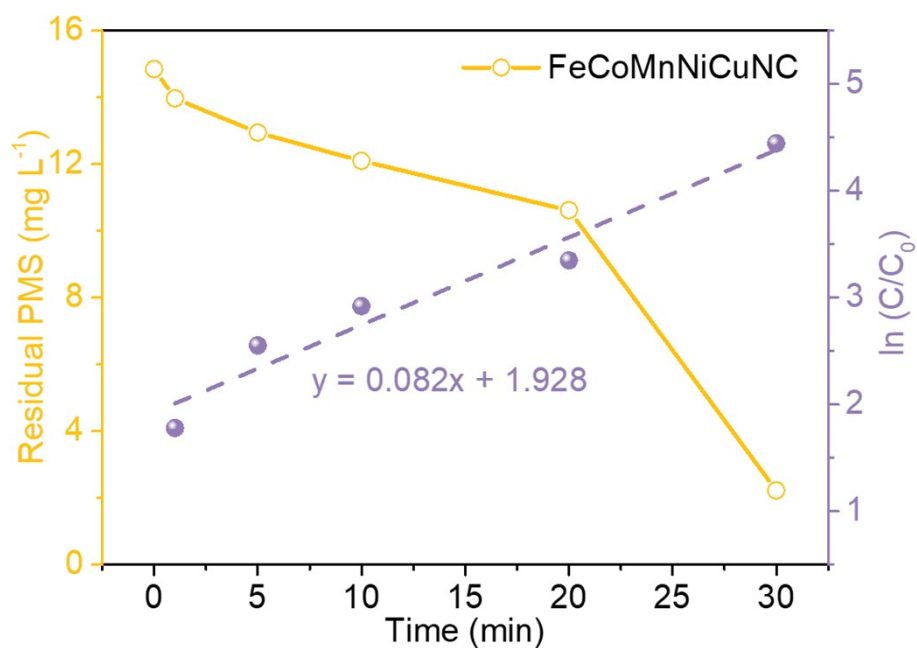


Figure S17. PMS consumption in BPA removal process by the FeCoMnNiCuNC. Reaction condition: [BPA] = 20 mg L⁻¹; [PMS] = 0.2 g L⁻¹ = 0.65 mM; [Cat] = 0.15 g L⁻¹; initial pH= 3.6, T = 298 K.

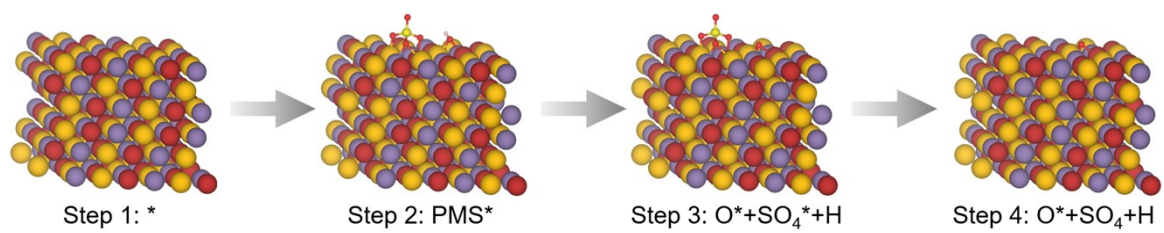


Figure S18. Reaction pathways of PMS activation at the FeCoMn sites.

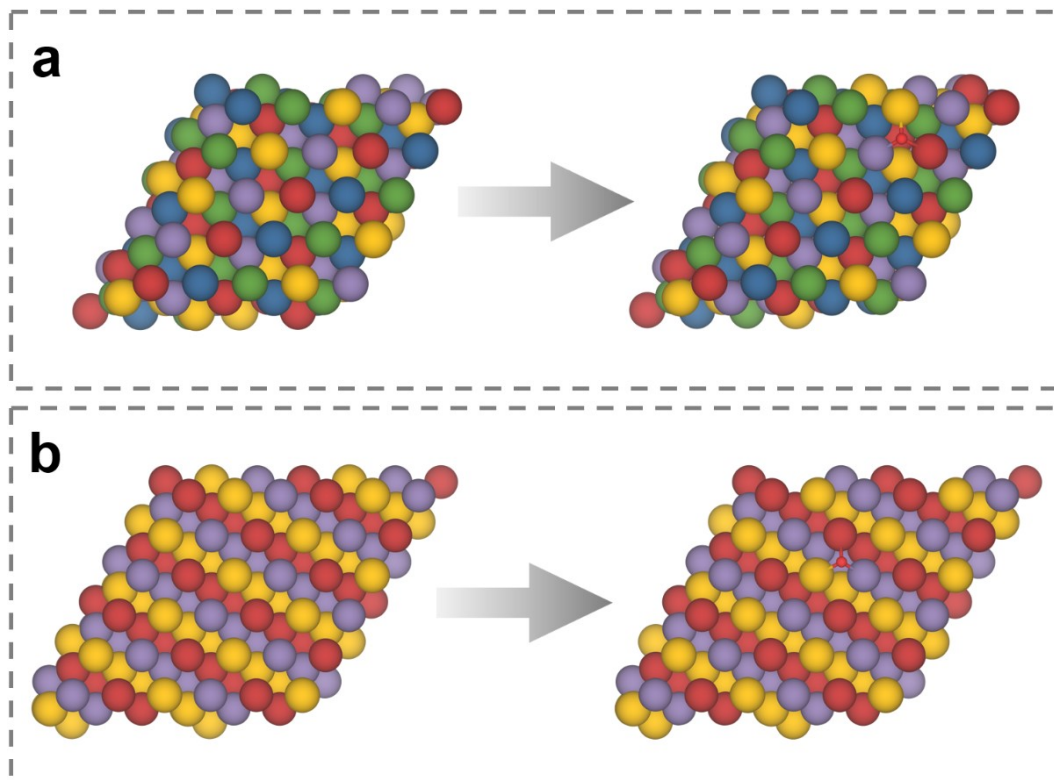


Figure S19. The atomic configurations on (a) FeCoMnNiCu; (b) FeCoMn.

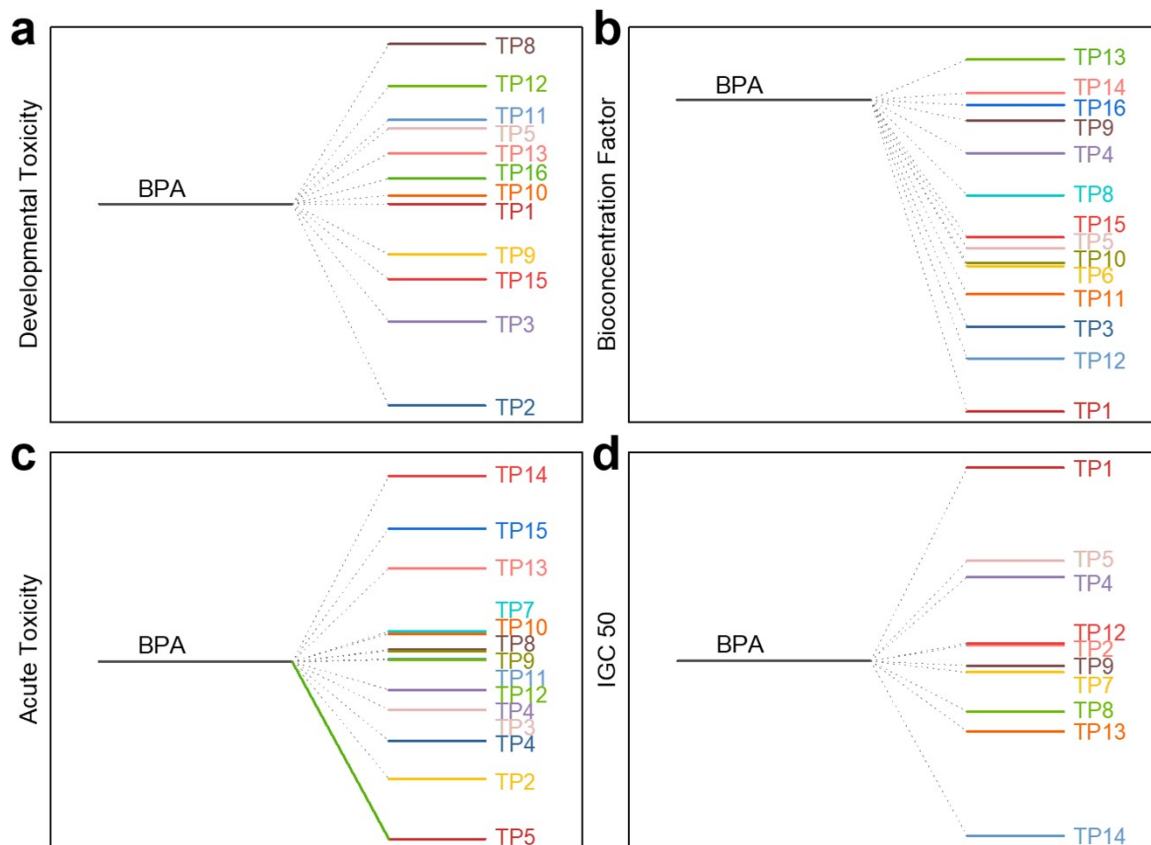


Figure S20. (a) Developmental toxicity, (b) bioconcentration factor, (c) acute toxicity (d) IGC 50 of BPA and its degradation intermediates.

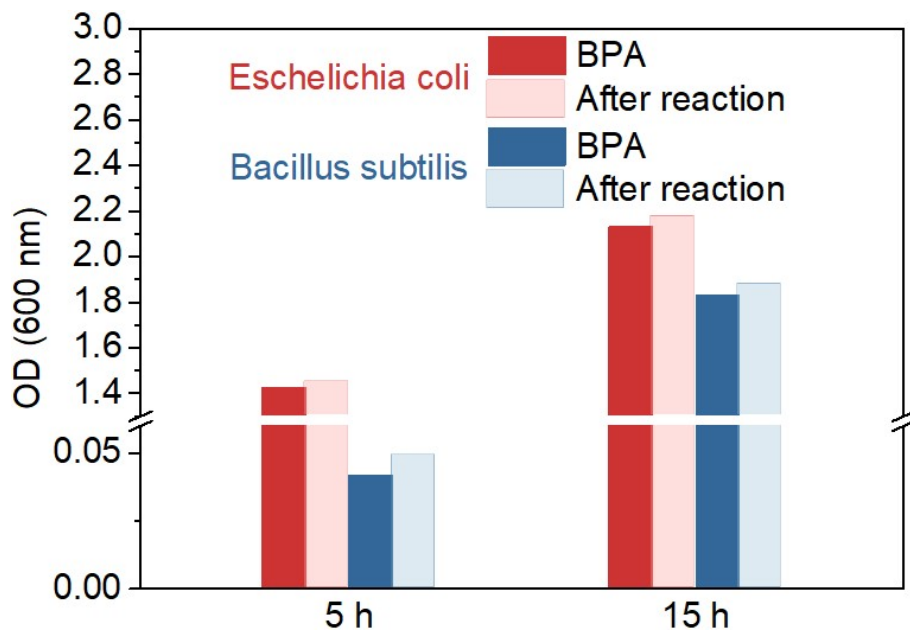


Figure S21. The growth situation of *Escherichia coli* and *Bacillus subtilis* in BPA and the treated BPA solution, respectively.

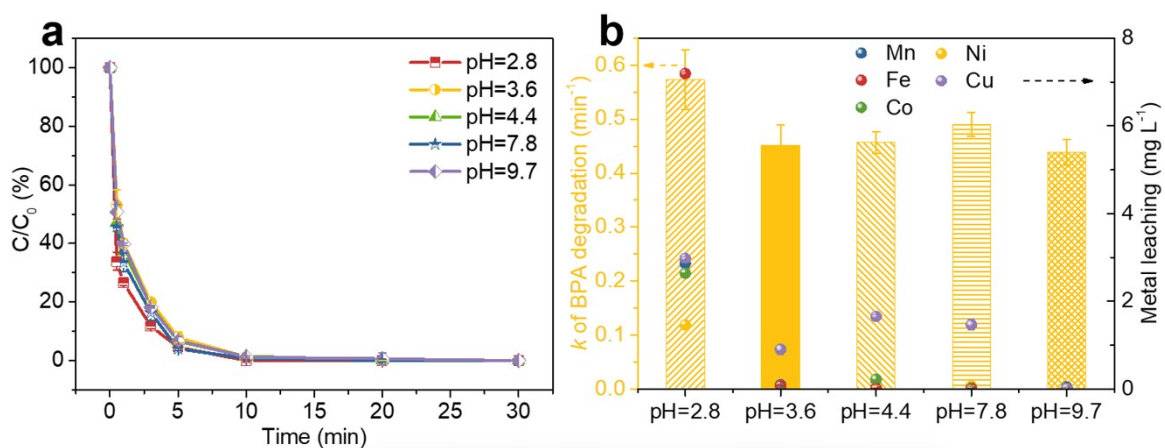


Figure S22. (a) BPA removal in PMS-activated process and (b) *k* of BPA degradation by the FeCoMnNiCuNC in different pH. Conditions: [BPA] = 20 mg L⁻¹; [PMS] = 0.2 g L⁻¹; [Cat] = 0.15 g L⁻¹; T = 298 K.

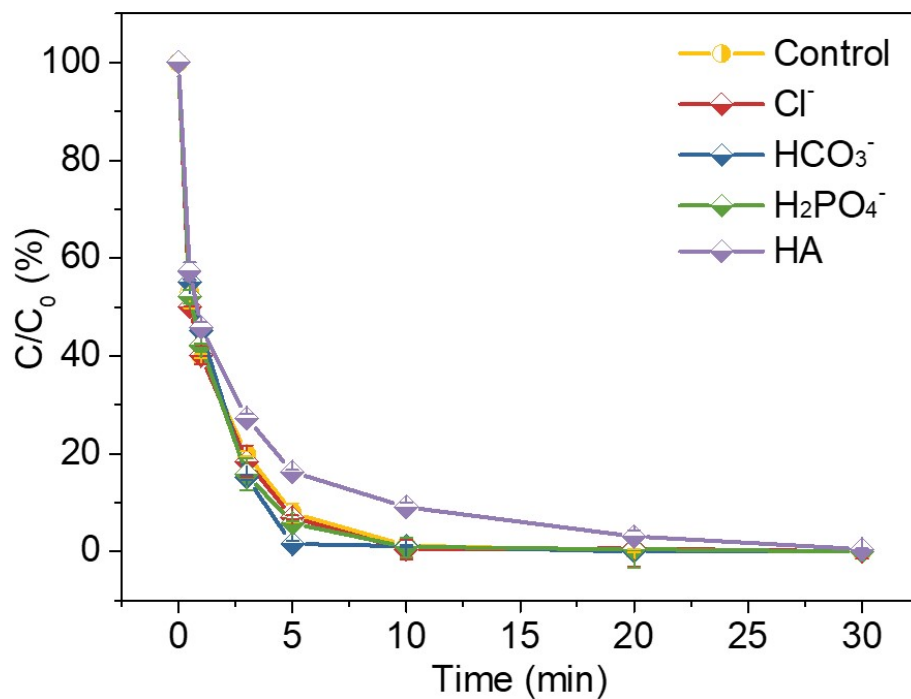


Figure S23. Impact of anions and natural organic matter. Condition: [BPA] = 20 mg L⁻¹; [PMS] = 0.2 g L⁻¹; [Cat] = 0.15 g L⁻¹; [Anions] = 20 mM; [HA] = 10 mM; initial pH= 3.6, T = 298 K.

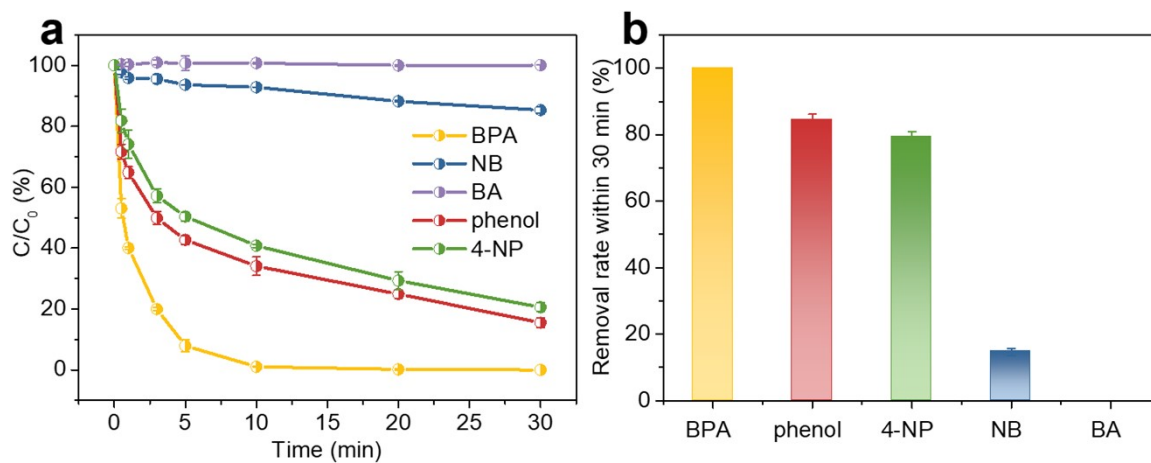


Figure S24. (a) Pollutants removal and (b) removal rate by the FeCoMnNiCuNC-activated PMS system. Condition: [PMS] = 0.2 g L⁻¹; [Cat] = 0.15 g L⁻¹; [Pollutants] = 20 mg L⁻¹; initial pH= 3.6, T = 298 K.

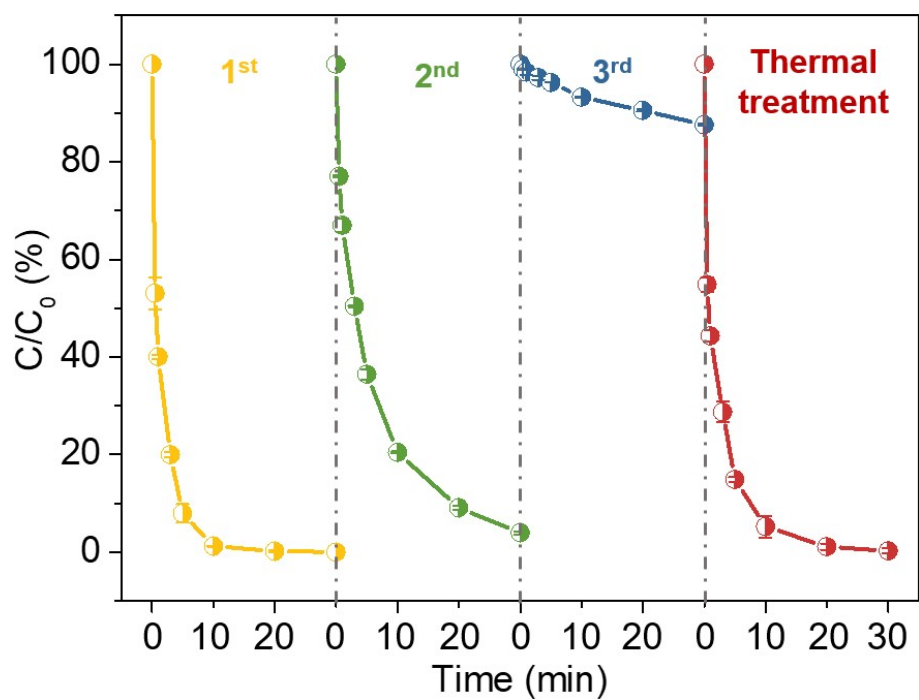


Figure S25. Recycle tests of the FeCoMnNiCu/PMS system. Condition: [BPA] = 20 mg L⁻¹; [PMS] = 0.2 g L⁻¹; [Cat] = 0.15 g L⁻¹; initial pH= 3.6, T = 298 K.

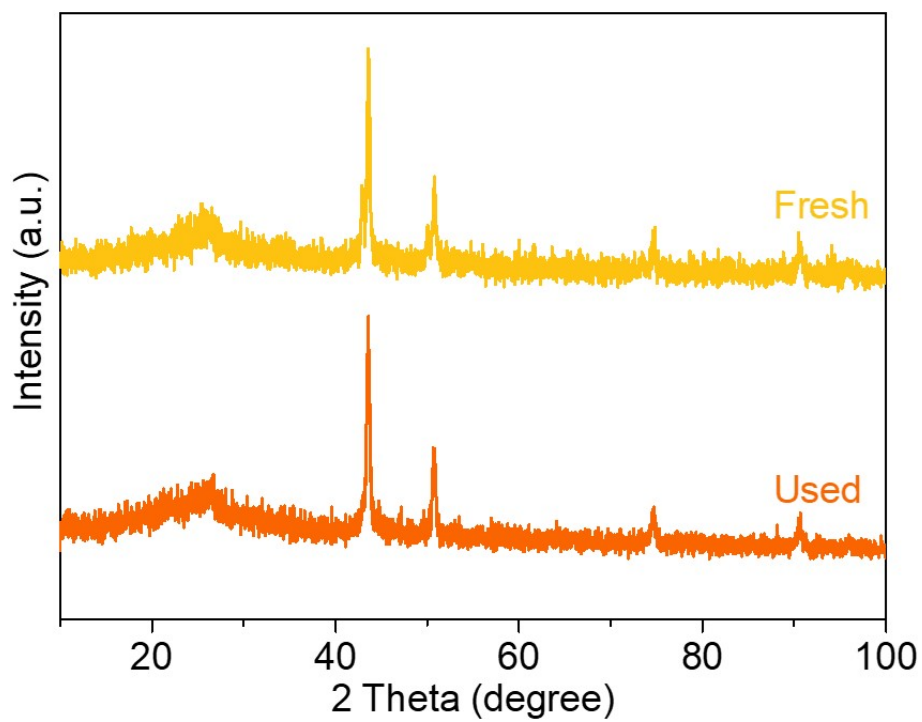


Figure S26. XRD patterns of FeCoMnNiCuNC before and after reaction.

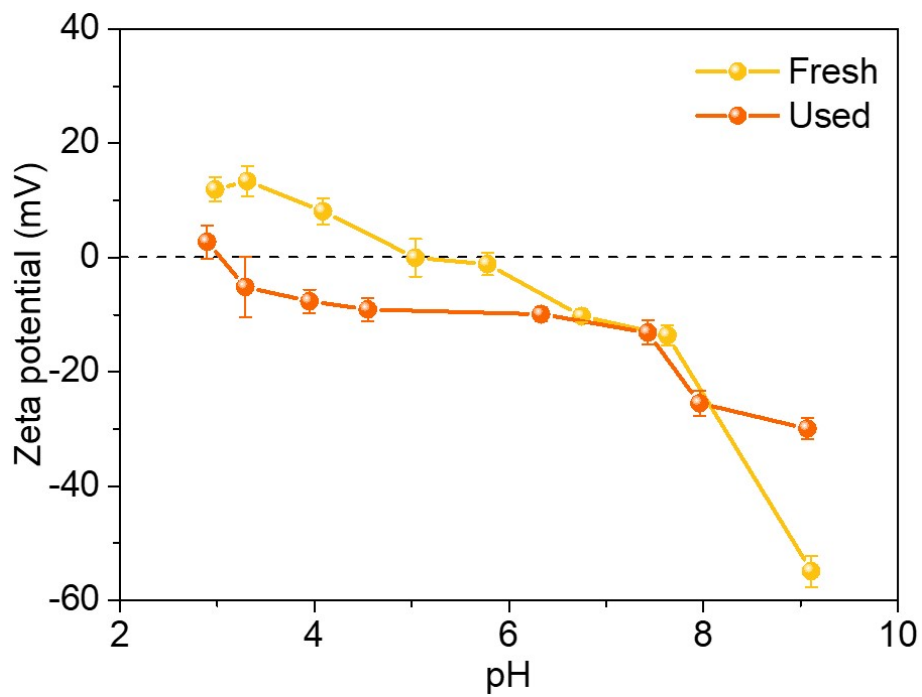


Figure S27. Zeta potential of FeCoMnNiCuNC before and after reaction.

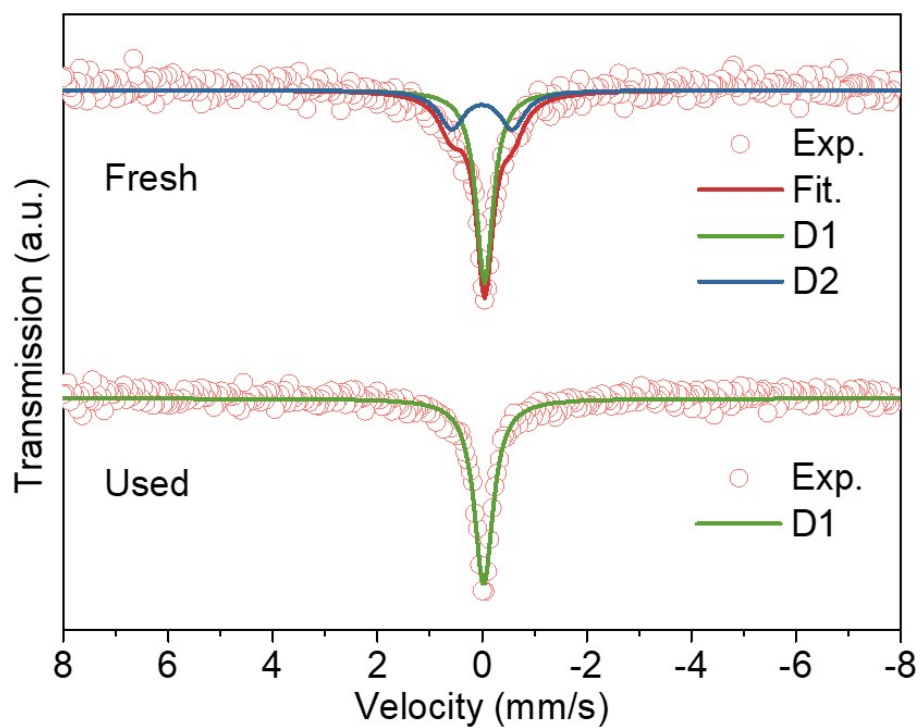


Figure S28. The ^{57}Fe Mössbauer spectra and fitting results of FeCoMnNiCuNC before and after reaction.

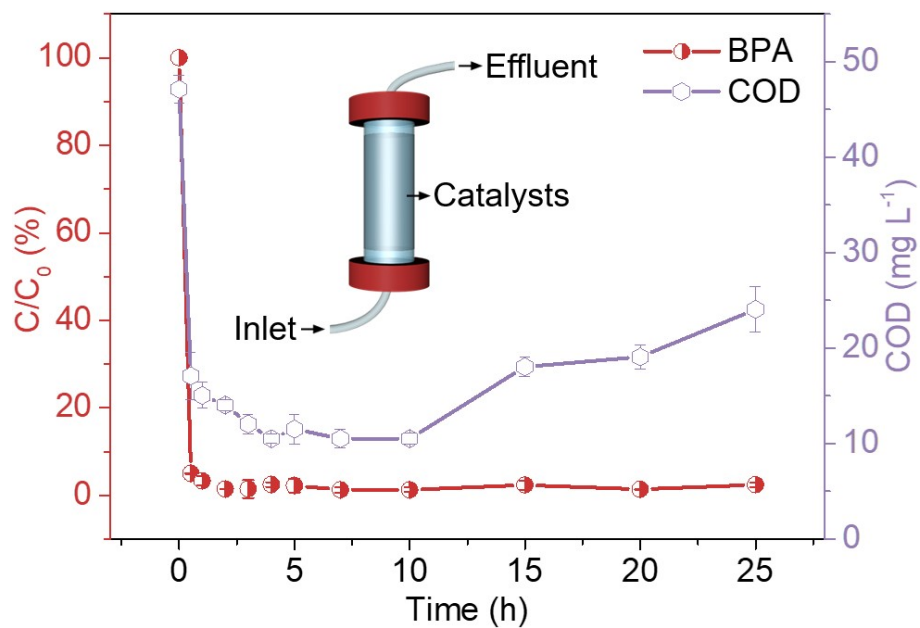


Figure S29. A column reactor for treatment of BPA-containing wastewater.

As displayed by Fig. S29 inset, the performance was tested for the continuous actual wastewater (secondary effluent of the Changzhou Wastewater Treatment Plant) decontamination under a hydraulic reaction time of ~ 16.5 min (flow rate: ~ 2.7 mL min $^{-1}$). A mixed solution of 50 mg L $^{-1}$ COD value with 10 mg L $^{-1}$ BPA and 0.02 mg L $^{-1}$ PMS was passed through the column, which contains 150 mg catalysts.

Table S1 The metal contents of different samples by ICP-OES.

Samples	Fe (mg L⁻¹)	Co (mg L⁻¹)	Mn (mg L⁻¹)	Ni (mg L⁻¹)	Cu (mg L⁻¹)
FeCoNC	11.06	15.11	/	/	/
FeMnNC	9.95	/	10.24	/	/
FeNiNC	9.75	/	/	14.00	
FeCuNC	9.94	/	/	/	15.14
FeCoMnNC	12.00	7.16	7.29	/	/
FeCoNiNC	16.52	13.34	/	13.28	/
FeCoCuNC	12.48	8.19	/	/	9.55
FeMnNiNC	17.80	/	13.85	14.67	/
FeMnCuNC	15.58	/	10.38	/	11.27
FeNiCuNC	14.37	/	/	10.26	9.30
FeCoMnNiNC	9.37	5.45	5.28	5.38	/
FeCoMnCuNC	9.17	5.05	5.01	/	5.52
FeCoNiCuNC	9.43	5.64	/	5.45	5.82
FeMnNiCuNC	9.25	/	5.63	5.29	5.49
FeCoMnNiCuNC	9.30	5.03	5.51	5.01	5.01
FeCoMnNiCuNC-used	9.16	5.01	5.22	5.00	4.99

Table S2 Textural properties of the samples.

Samples	Surface Area (m² g⁻¹)	Pore Volume (cm³ g⁻¹)
FeCoNC	157.2	0.31
FeCoMnNC	203.9	0.38
FeCoMnCuNC	155.5	0.32
FeCoMnNiCuNC	123.8	0.26
FeCoMnNiCu-PBAs-C	22.2	0.06

Table S3 Catalytic performance comparison of recently reported catalysts for BPA removal.

Type of catalyst	Catalyst (g L ⁻¹)	PMS (g L ⁻¹)	BPA (mg L ⁻¹)	<i>k</i> (min ⁻¹)	Removal rate% / Time (min)	Ref.
Metal oxide	Mn _{1.8} Fe _{1.2} O ₄ (0.1)	0.20	10	0.10	95/30	2
Metal oxide	ZnFeMnO ₄ (0.1)	0.02	10	0.09	100/15	3
Metal/carbon	Fe ₁ Mn ₅ Co ₄ -N@C (0.1)	0.20	20	0.48	100/12	4
O _v	Ovc-CNOP Nfs (0.8)	3.10	10	0.07	100/1	5
Single-atom	Fe-SAC (0.1)	0.4	25	0.10	88/30	6
Single-atom	Co-SAC (0.1)	0.4	25	0.08	79/30	6
Single-atom	Fe-N-C (0.1)	0.03	22.8	0.27	100/10	7
Single-atom	FeN _x -C-600 (0.2)	0.03	20	0.36	97.9/15	8
Doping	Fe ₂ P-NPs/NC (0.1)	0.15	10	0.62	100/30	9
Doping	Cu-N ₄ /C-B (0.1)	0.20	20	0.56	98/5	10
Doping	Cu-N ₄ /C-P (0.1)	0.20	20	0.01	11/5	10
Dual-atom	MCNC (0.03)	0.10	20	0.14	100/30	11
Alloy	FeCoNC (0.2)	0.15	20	0.15	79.81/10	This work
Alloy	FeCoMnNC (0.2)	0.15	20	0.37	96.74/10	This work
Alloy	FeCoMnCuNC (0.2)	0.15	20	0.43	98.70/10	This work
High entropy alloy	FeCoMnNiCuNC (0.2)	0.15	20	0.45	98.97/10	This work

Table S4 Structures and HPLC analytical methods of various pollutants.

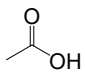
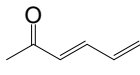
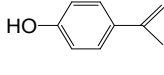
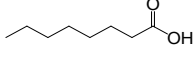
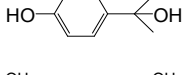
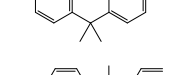
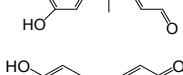
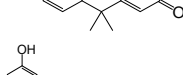
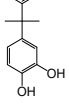
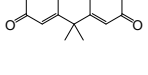
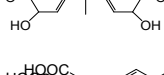
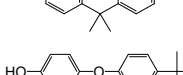
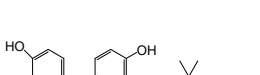
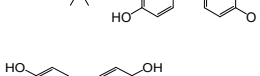
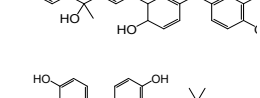
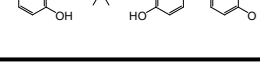
Nam e	Proposed structure	Molecular formula	Time (min)	MS/MS (m/z)	MS (m/z)	Erro r
TP-1		C ₂ H ₄ O ₂	5.15	59.0139	59.0135	-6.8
TP-2		C ₆ H ₈ O	5.859	95.05024	95.0504	1.7
TP-3		C ₉ H ₁₀ O	3.607	133.0659	133.0659	0
TP-4		C ₈ H ₁₆ O ₂	5.11	143.1078	143.1076	1.4
TP-5		C ₉ H ₁₂ O ₂	5.654	151.07645	151.0765	3.3
TP-6		C ₁₅ H ₁₆ O ₂	5.076	227.1078	227.1079	-0.4
TP-7		C ₁₄ H ₁₆ O ₃	3.607	231.10267	231.1032	2.3
TP-8		C ₁₅ H ₁₄ O ₃	5.851	241.08702	241.0869	-0.5
TP-9		C ₁₅ H ₁₆ O ₃	4.432	243.1027	243.1027	-0.8
TP-10		C ₁₅ H ₁₂ O ₄	4.668	255.06628	255.06624	-4.3
TP-11		C ₁₅ H ₁₄ O ₄	3.824	257.09758	257.0962	-5.3
TP-12		C ₁₅ H ₁₆ O ₅	3.635	275.0925	275.0936	4
TP-13		C ₂₁ H ₂₀ O ₃	6.467	319.134	319.1333	-2.2
TP-14		C ₃₀ H ₃₀ O ₄	6.647	453.20713	453.2052	-4.3
TP-15		C ₃₀ H ₃₀ O ₅	6.041	469.20205	469.2012	-1.8
TP-16		C ₃₇ H ₃₆ O ₅	7.932	559.249	559.2474	-2.9

Table S5 Fitting parameters for the ^{57}Fe Mössbauer spectra of the FeCoMnNiCuNC before and after reaction.

Sample	Component	IS (mm s⁻¹)	QS (mm s⁻¹)	Hhf (kOe)	Area (%)	Assignment
Fresh	D1	-0.05	-	-	63.6	Fe ⁰
	D2	0.003	1.16	-	36.4	Alloyed Fe ⁰
Used	D1	-0.03	-	-	100	Fe ⁰

S is the isomer shift, QS is the quadrupolar splitting, and Hhf is the hyperfine magnetic field.

References

- 1 Y. Wang, J. Le Roux, T. Zhang and J. P. Croue, *Environ. Sci. Technol.*, 2014, **48**, 14534-14542.
- 2 G.-X. Huang, C.-Y. Wang, C.-W. Yang, P.-C. Guo and H.-Q. Yu, *Environ. Sci. Technol.*, 2017, **51**, 12611-12618.
- 3 Z.-Y. Guo, Y. Si, W.-Q. Xia, F. Wang, H.-Q. Liu, C. Yang, W.-J. Zhang and W.-W Li, *Proc. Natl. Acad. Sci. U.S.A.*, 2022, **119**, e2201607119.
- 4 X. Li, Z. Ao, J. Liu, H. Sun, A. I. Rykov and J. Wang, *ACS Nano*, 2016, **10**, 11532-11540.
- 5 W. Cao, L. Lyu, K. Deng, C. Lu and C. Hu, *J. Mater. Chem. A*, 2020, **8**, 810-819.
- 6 Y. Gao, T. Wu, C. Yang, C. Ma, Z. Zhao, Z. Wu, S. Cao, W. Geng, Y. Wang, Y. Yao, Y. Zhang and C. Cheng, *Angew. Chem. Int. Ed.*, 2021, **60**, 22513-22521.
- 7 C. Cheng, W. Ren, F. Miao, X. Chen, X. Chen and H. Zhang, *Angew. Chem. Int. Ed.*, 2023, **62**, e202218510.
- 8 B. Zhang, X. Li, K. Akiyama, P.A. Bingham and S. Kubuki, *Environ. Sci. Technol.*, 2021, **56**, 1321-1330.
- 9 Z. Yang, X. Yang, G. An and D. Wang, *Appl. Catal. B: Environ.*, 2023, **330**, 122618.
- 10 X. Zhou, M.-K. Ke, G.-X. Huang, C. Chen, W. Chen, K. Liang, Y. Qu, J. Yang, Y. Wang, F. Li, H.-Q. Yu and Y. Wu, *Proc. Natl. Acad. Sci. U.S.A.*, 2022, **119**, e2119492119.
- 11 Y. Yao, C. Wang, Y. Yang, S. Zhang, X. Yan, C. Xiao, Y. Zhou, Z. Zhu, J. Qi, X. Sun and J. Li, *Appl. Catal. B: Environ.*, 2023, **330**, 122656.